Oxygen intercalation, stage ordering, and phase separation in $La_2NiO_{4+\delta}$ with $0.05 \lesssim \delta \lesssim 0.11$

J. M. Tranquada, Y. Kong,* and J. E. Lorenzo
Physics Department, Brookhaven National Laboratory, Upton, New York 11973

D. J. Buttrey, D. E. Rice, and V. Sachan
Department of Chemical Engineering, University of Delaware, Newark, Delaware 19716
(Received 29 March 1994)

We report neutron diffraction studies on a series of $La_2NiO_{4+\delta}$ single crystals with $0.05 \lesssim \delta \lesssim 0.11$. At 300 K, all of the crystals have an average tetragonal structure (space group $I4/mmm$). On cooling below 290 K, one or more orthorhombic phases appear, characterized by incommensurate superlattice peaks at $(0, k, l \pm \Delta)$ with k odd, l even, and $\frac{1}{4} < \Delta \leq \frac{1}{2}$. The positions, widths, and intensities of the superlattice peaks are quite sensitive to the cooling rate. We show that the incommensurate peaks are evidence of intercalated layers of oxygen spaced periodically along the c axis, with a one-dimensional ordering similar to the staging of intercalates in graphite. The structure of the La_2NiO_4 lattice between the interstitial layers is of the *Bmab*-type; the superlattice peaks result from the ordered antiphase domain boundaries induced by the interstitial oxygens, which sit at $(\frac{1}{4}, \frac{1}{4}, \frac{1}{4})$-type positions. Observed orderings involve interstitial layers separated by two to four Ni-O layers. Peak shapes and positions are modelled quantitatively using the formulas of Hendricks and Teller for one-dimensional disorder in a layer lattice. Besides the one-dimensional ordering of the intercalant layers, temperature-dependent phase separations are observed. Because of the slow ordering kinetics, phase separation can be suppressed by rapid cooling.

I. INTRODUCTION

An issue of significant interest for understanding the electronic and magnetic behaviors of doped La_2NiO_4 and La_2CuO_4 concerns the degree of ordering of the dopant ions. Doping holes into La_2CuO_4, either by substituting alkaline earth ions (Sr^{2+}, Ba^{2+}, or Ca^{2+}) for La^{3+} or by adding excess oxygen, leads to a metallic, superconducting phase.[1,2] While the alkaline earth ions become immobile at relatively high temperatures, the interstitial oxygens remain mobile even below room temperature, and have a tendency to phase separate.[3–5] Phase separation is also a well-established phenomenon in nonmetallic, nonsuperconducting $La_2NiO_{4+\delta}$.[6–8]

Much of the diffraction work on $La_2NiO_{4+\delta}$ and $La_2CuO_{4+\delta}$ has involved polycrystalline samples. In such studies, phase separation can be identified fairly directly from the splitting of fundamental Bragg peaks. The ordering of oxygen interstitials, on the other hand, is somewhat more difficult to establish, as it requires the detection of very weak superlattice reflections. Individual added oxygens tend to sit between adjacent LaO layers, as shown by Jorgensen *et al.*[9] in $La_2NiO_{4+\delta}$ and by Chaillout and co-workers[10,11] in $La_2CuO_{4+\delta}$. The first evidence for ordering of the oxygens came from an electron diffraction study of $La_2NiO_{4+\delta}$ with $0.04 \lesssim \delta \lesssim 0.20$ by Hiroi *et al.*,[12] who observed superlattice peaks that suggested three-dimensional order involving very large unit cells. They speculated that ordered phases occur when the oxygen excess, δ, is equal to $1/2n$, where n is an integer greater than 1. More recently, Demourgues *et al.*[13,14] have used electron diffraction to identify a new monoclinic, oxygen-ordered phase at $\delta = 0.25$; the structure was refined using neutron powder diffraction measurements. Evidence for a large superstructure in $La_2CuO_{4+\delta}$ with $\delta \approx 0.1$ has been observed in a single-crystal neutron diffraction study by Radaelli *et al.*[15]

In the present paper we describe a neutron diffraction study of oxygen ordering in a series of single crystals of $La_2NiO_{4+\delta}$ with well-characterized oxygen contents in the range $0.05 \lesssim \delta \lesssim 0.11$. We show that, contrary to the conclusions of Hiroi *et al.*,[12] the interstitial oxygens in bulk crystals order only one dimensionally, in layers ordered periodically along the c axis. Our conclusions are derived from the analysis of superlattice peaks that appear below 290 K at the positions $(0, k, l \pm \Delta)$, with k odd, l even, and $\frac{1}{4} < \Delta \leq \frac{1}{2}$. Such peaks, with $\Delta = \frac{1}{2}$, were first observed in an earlier study[16] on the $\delta = 0.105$ crystal, but their significance was misinterpreted. Here we show that the positions, widths, and intensities of the peaks can be quantitatively interpreted using a model in which the interstitials cluster in layers that form antiphase-domain boundaries in a lattice with local *Bmab* symmetry. The ordering of the layers is quite similar to the staging of alkali atoms intercalated in graphite.[17] An important distinction from intercalated graphite, however, is that we have observed a temperature-dependent phase separation into two phases with different stagings.

In the hope that it will make the discussion of the data more understandable, we begin the paper by describing the model for the intercalated structure, and

how it can be related to the diffraction measurements using the Hendricks-Teller formulas for random ordering in a layer-type lattice. The experimental procedure is described in Sec. III. The presentation of the data and analysis follow in Sec. IV; this includes results on the magnetic ordering of the Ni moments. The paper concludes with a summary and discussion in Sec. V.

II. MODEL

A. Oxygen intercalation

At high temperatures, La_2NiO_4 has the body-centered tetragonal K_2NiF_4 structure (also known as HTT, for high-temperature tetragonal), consisting of sheets of corner-sharing NiO_6 octahedra (elongated perpendicular to the sheets). The La ions are positioned in the layers formed by the apical oxygens. Because of the body centering, there are two Ni-O layers per unit cell. In the following discussion, we will assume that distortions of the Ni-O layers consist of rotations of the relatively rigid NiO_6 octahedra, with no displacements of the Ni ions. If we tilt one octahedron about a [110] axis of the tetragonal unit cell, then the apical oxygens will be displaced along $[1\bar{1}0]$. The in-plane oxygens are displaced perpendicular to the plane, and because they are shared with four neighboring octahedra, these nearest-neighbor octahedra will rotate in the opposite direction. In such a fashion, the distortion will propagate throughout the plane. Because the pattern is antiferrodistortive, the unit cell size is doubled. The sides of the $\sqrt{2} \times \sqrt{2}$ unit cell have slightly different lengths; it is the axis *along* the tilt direction which becomes the longer one, contrary to what one would expect for perfectly rigid octahedra. This tilt pattern occurs in the room-temperature structures of La_2NiO_4 and La_2CuO_4 (space group *Bmab*), commonly referred to as low-temperature orthorhombic (LTO).

Jorgensen *et al.*[9] suggested that an interstitial oxygen should sit in the $(\frac{1}{4}, \frac{1}{4}, \frac{1}{4})$ position of the orthorhombic unit cell, directly above an in-plane oxygen and symmetrically positioned among four La ions and four apical oxygens. Such an interstitial will repel the nearest-neighbor oxygens. Suppose that the apical neighbors are displaced away from the interstitial along the orthorhombic [010] direction (equivalent to the tetragonal $[1\bar{1}0]$). The tilts would then propagate within the planes, and assuming that they also propagate perpendicular to the planes (due to Coulomb interactions or other effects), one would find the *Bmab* tilt pattern above and below the plane of the interstitial. However, this accommodation of the interstitial involves a reversal of the usual *Bmab* tilt pattern on crossing the plane of the interstitials. This is illustrated in Fig. 1, where the displacements of the apical oxygens in the layers immediately adjacent to the interstitial plane are indicated for both the normal and intercalated *Bmab* lattices. Thus, the interstitial layer creates an antiphase domain boundary. Note that the tilt pattern in the intercalated phase creates an entire array of favorable interstitial positions, whereas none exist in the normal *Bmab* phase. Hence, it appears that once one interstitial occupies a $(\frac{1}{4}, \frac{1}{4}, \frac{1}{4})$ position in a particular layer, it will be energetically favorable for other oxygen atoms to occupy the same layer.

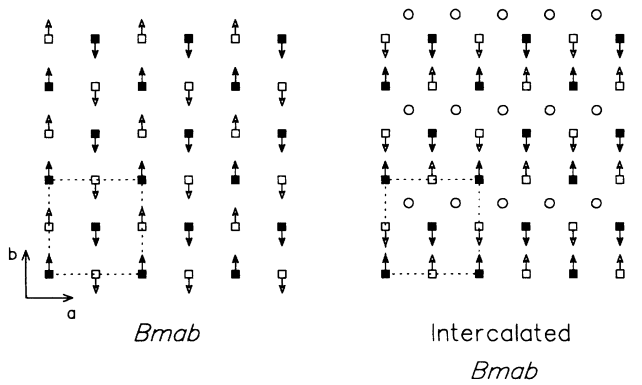

FIG. 1. Displacement patterns of apical oxygens located immediately above and below an interstitial layer in the normal and intercalated *Bmab* phases. The open (solid) squares represent apical oxygens hanging down (sticking up) from the Ni-O plane above (below). The arrows indicate the directions of displacement, and the dotted lines indicate the size of the orthorhombic unit cell. The open circles in the right-hand figure indicate favorable interstitial positions.

Of course, if the interstitial oxygens grab electrons from the lattice to fill their $2p$ shells, they will become charged. The Coulomb repulsion between ionic interstitials will limit the density within an interstitial layer, and also the spacing of intercalated layers along the c axis. In the case of alkali metals intercalated in graphite, the long-range repulsive interaction between layers leads to a periodic ordering of the alkali layers.[17] We will show that a similar periodic ordering of intercalated oxygen layers occurs in $La_2NiO_{4+\delta}$ over a significant range of δ. To describe the ordering it is convenient to adopt the notion of "staging" developed for intercalated graphite. A stage n ordering consists of single interstitial oxygen layers separated by n Ni-O planes. Examples of stage-4, -3, and -2 orderings are illustrated in Fig. 2.

In the samples where we have observed staging of the interstitials, the oxygen density within an interstitial layer is fairly low, and we have not detected any evidence for long-range intralayer order of the added oxygens. Instead, the ordering of the layers manifests itself through the tilt pattern of the NiO_6 octahedra (and the concomitant displacements of the La ions). As noted above, we assume a tilt pattern identical to that of the *Bmab* phase between interstitial layers, with the tilt direction reversing on crossing an interstitial layer. Thus, the period of the structure along the c direction is not the spacing between the intercalant layers, but twice that. We have studied the resulting superlattice peaks that appear in the $(0kl)$ zone. [It should be noted that because of twinning, we sample the $(h0l)$ and $(0kl)$ zones simultaneously.] The reflections observed in the combined $(h0l)/(0kl)$ zones for stage-2 order are indicated in Fig. 3. For the pure *Bmab* phase, superlattice peaks

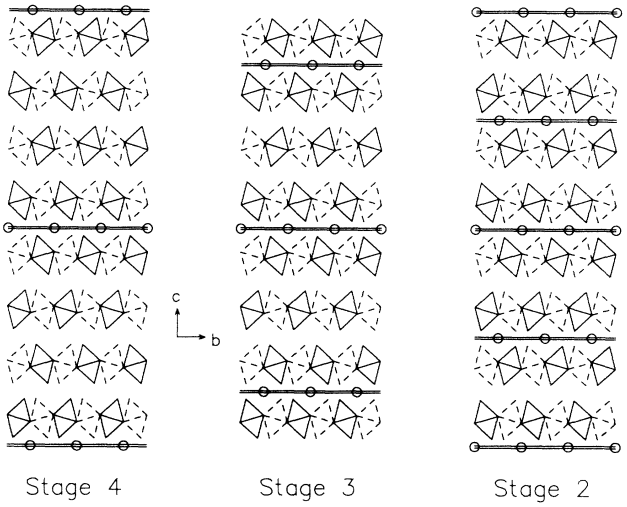

FIG. 2. Tilt patterns of the NiO_6 octahedra for various stagings of the interstitial oxygen layers. The central axes of the solid octahedra lie in the plane of the figure, while those of the dashed octahedra are displaced perpendicular to that plane by $\frac{1}{2}a$. The interstitial positions, indicated by open circles, are displaced by $\frac{1}{4}a$. The magnitude of the tilts is exaggerated for clarity.

appear for the conditions k odd, l even and not equal to zero. For an ideal stage-n intercalated *Bmab* phase, the superlattice peaks should appear at $(0, k, l \pm \frac{1}{n})$ with k odd and l even (including zero). The actual peaks observed for intercalated samples rarely occur at precisely these positions. The peak displacements occur due to imperfect ordering as we discuss next.

Before discussing stacking disorder, we wish to emphasize that by introducing the name "intercalated *Bmab*" we do not mean to imply that the correct space group for the staged structures is *Bmab*. Rather, we intend the name to indicate that the tilt pattern between the interstitial layers is of the *Bmab* type, with octahedral tilts about a tetragonal [110] axis, as opposed, for example, to the tilts about a tetragonal [100] axis that occur in the space group $P4_2/ncm$. The overall staged structure can be considered to be a *Bmab*-type lattice with an ordered array of antiphase domain boundaries. The positions of the superlattice peaks are controlled by the domain boundary spacing. Of course, the interstitials also cause a slight expansion of the occupied La_2O_2 layers relative to the unoccupied ones, which breaks the *B*-centered symmetry for the Ni sites. (This symmetry is already broken for the O and La sites by the octahedral tilt reversal across the interstitial layers.)

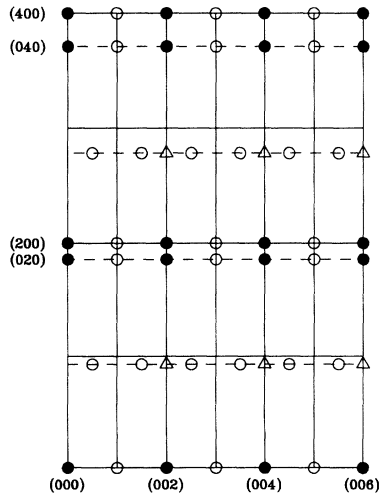

FIG. 3. Schematic diagram of the $(h0l)$ and $(0kl)$ zones, which are sampled simultaneously due to twinning. The orthorhombic splitting is greatly exaggerated for clarity. Solid circles represent the fundamental reflections of the undistorted $F4/mmm$ structure. Open triangles indicate superlattice peaks expected for the *Bmab* phase, while open circles indicate those observed for the stage-2 intercalated *Bmab* phase.

B. Ordering of intercalated phases

We have described an idealized ordering of the interstitial oxygen which we will use as the basis for analyzing the observed scattering patterns. However, the real crystals tend to exhibit much more disorder than suggested above. There are several factors responsible for the disorder. For one thing, the oxygen is loaded into the crystals at relatively high temperatures, where the oxygen is diffusing rapidly and ordering effects are weak. Next, as a crystal is cooled, ordering requires a rearrangement of the oxygen interstitials. Assuming that an interstitial can move only parallel to a layer, and not hop between layers, one may expect the oxygens to order in metastable structures, with large energy barriers for reaching the lowest-energy, well-ordered states. Finally, an arbitrary oxygen content δ will not necessarily correspond to a unique staging, and hence phase separation may occur. The ordering kinetics are quite slow, and we will show that the measurements are quite sensitive to the rate of sample cooling and heating.

The point to be made here is that one must allow for the disorder in modeling the experimental measurements. Similar disorder effects have been analyzed previously in diffraction studies of intercalated graphite.[18,19] The disorder does not invalidate the underlying model, although it has caused us considerable confusion in identifying it. The disorder merely adds some complexity to the analysis.

C. LTT phase

Before turning to the problem of calculating the scattering from the disordered intercalated phases, we wish to point out that intercalation does not explain the behavior of the interstitials all the way down to $\delta = 0$. A low-temperature tetragonal (LTT) phase (space group $P4_2/ncm$) intervenes for $0.02 \lesssim \delta \lesssim 0.03$.[6] In this structure the NiO_6 octahedra rotate by equal amounts about the [110] and [1$\bar{1}$0] axes of the simple tetragonal cell, doubling the in-plane unit cell as in the LTO case. The net tilt direction is along a [110] axis of the $\sqrt{2} \times \sqrt{2}$ cell, and it rotates by 90° in the neighboring layers.

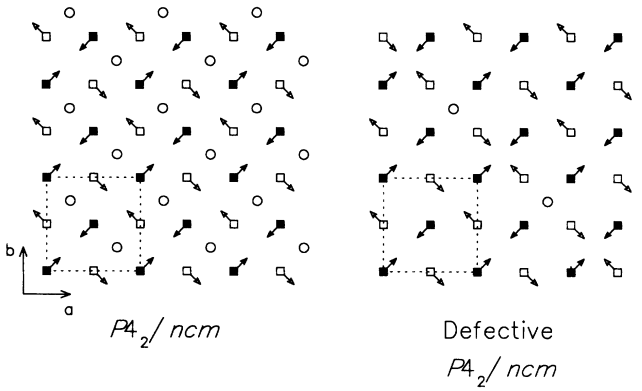

FIG. 4. Same as Fig. 1, but for the $P4_2/ncm$ phase. For the defective phase, the displacements of the central diagonal row of open squares has been reversed, creating especially favorable interstitial positions, indicated by open circles.

The displacements of the apical oxygens neighboring a $\frac{1}{4}c$ interstitial layer in the LTT phase are shown in Fig. 4. For half of the $(\frac{1}{4},\frac{1}{4},\frac{1}{4})$ positions, the neighboring oxygens are rotated transversely in a symmetric fashion. Such positions, with some extra displacement locally, might accommodate isolated interstitials. An alternative possibility is shown in the right-hand side of the figure. Axe[20] has pointed out that, since only half of the in-plane oxygens are displaced in the LTT octahedral tilt pattern, it is possible to flip the tilts of a diagonal row of octahedra without disturbing the neighboring rows. Such a defect row creates interstitial positions in which, at least in projection, all neighboring oxygens are displaced radially away from the interstitial site. These sites would be quite favorable for the added oxygens. In any case, we have not detected any long-range ordering of the interstitials in this phase.

D. Scattering calculations

As we have noted above, it is necessary to take into account disorder in the stacking of the intercalated layers when interpreting the data. The problem of scattering from a lattice consisting of two or more types of layers with a random ordering was first treated by Hendricks and Teller.[21] Suppose that we have N types of layers, and that the structure factor of the nth type is $F_n(\mathbf{Q})$. The nth type of layer occurs with frequency f_n, and

$$\sum_{n=1}^{N} f_n = 1. \tag{1}$$

The result for the scattered intensity can be expressed rather succinctly[22] if we define the quantities G and $V_\pm$ such that

$$G(\mathbf{Q}) = \sum_{n=1}^{N} f_n e^{-i2\phi_n}, \tag{2}$$

$$V_\pm(\mathbf{Q}) = \sum_{n=1}^{N} f_n F_n e^{\pm i\phi_n}, \tag{3}$$

where the phase shift ϕ_n is given by

$$\phi_n = \mathbf{Q}\cdot\tilde{\mathbf{c}}_n/2, \tag{4}$$

with $\tilde{\mathbf{c}}_n$ being a vector perpendicular to the layers with a magnitude equal to the thickness of layer n. The scattered intensity is then given by

$$I = \sum_{n=1}^{N} f_n|F_n|^2 + 2\mathrm{Re}\left(\frac{V_+^* V_-}{1-G}\right). \tag{5}$$

Next, we must consider how to specify the layers for our model of oxygen intercalation. Since the scattering comes from the tilt pattern of the octahedra rather than from the interstitial oxygens themselves, it is important that for any possible stacking of the model layers the tilt direction is reversed every time an intercalated layer is crossed. This requirement can be enforced if we take as a scattering unit a stack of n Ni-O layers of one tilt domain, followed by m layers of the opposite domain type. Such a unit will be denoted by $n{:}m$. Thus, to describe a sample with a random mixture of stage-2 and stage-3 units, we will include the units 2:2, 2:3, 3:2, and 3:3. In principle, we need to specify the frequency of each layer combination, $f_{n:m}$, so that four parameters are required. However, combining the constraint given by Eq. (1) with the requirement $f_{n:m} = f_{m:n}$ reduces the number of parameters to 2, which we choose to be $f_{n:n}$ and $f_{m:m}$.

The structure factor $F_{n:m}$ for an $n{:}m$ scattering unit is fairly simple. Let F be the structure factor for a single Ni-O layer plus its associated La ions. Then

$$F_{n+1:n}/F = 1 + 2i\sum_{m=1}^{n}\sin(m\pi l), \tag{6}$$

$$F_{n:n}/F = 2i\sum_{m=1}^{n}\sin\left[(m-\tfrac{1}{2})\,\pi l\right], \tag{7}$$

$$F_{n:n+1}/F = -1 + 2i\sum_{m=1}^{n}\sin(m\pi l). \tag{8}$$

The structure factor for a single layer can be written as

$$F = F_{\mathrm{O}(1)} + F_{\mathrm{O}(2)} + F_{\mathrm{La}}, \tag{9}$$

where, for a $(0kl)$ zone with k odd,

$$F_{\mathrm{O}(1)} = 4b_{\mathrm{O}}\sin(\tfrac{\pi}{2}k)\sin(2\pi l z_{\mathrm{O}(1)}), \tag{10}$$

$$F_{\mathrm{O}(2)} = -4b_{\mathrm{O}}\sin(2\pi k y_{\mathrm{O}(2)})\sin(2\pi l z_{\mathrm{O}(2)}), \tag{11}$$

$$F_{\mathrm{La}} = -4b_{\mathrm{La}}\sin(2\pi k y_{\mathrm{La}})\sin\left[2\pi l\,(\tfrac{1}{2}-z_{\mathrm{La}})\right], \tag{12}$$

with b_{O} and b_{La} being the nuclear scattering amplitudes for oxygen and lanthanum. The O(1) atoms lie in the NiO_2 planes, and the O(2) sites are the apical positions. There are five structural parameters that must be specified. If one assumes that the octahedra rotate rigidly, then $z_{\mathrm{O}(1)}$ is determined once $y_{\mathrm{O}(2)}$ and $z_{\mathrm{O}(2)}$ are specified. Another constraint comes from the empirical

result[9,23] $y_{La} \approx -0.2y_{O(2)}$. One then has just three independent structural parameters: $y_{O(2)}$, $z_{O(2)}$, and z_{La}. For the calculations shown in the following sections, the values $y_{O(2)} = 0.05$, $z_{O(2)} = 0.16$, and $z_{La} = 0.37$ were used. The calculations extend over a very small range of **Q**, and so are not very sensitive to the particular values used.

To get a good quantitative fit to the data it is necessary to take into account the effects of resolution. This was done by convolving the calculated structure factor with a Gaussian, whose width corresponds to the experimental resolution.

III. EXPERIMENTAL PROCEDURE

The crystals used in this study were obtained by congruent melt growth using radio-frequency induction skull melting, as discussed in detail elsewhere.[6] The annealing conditions used to obtain the various oxygen excesses are also described in that reference. Previous work[6] has determined the correlation between the c/a ratio and δ, with the latter determined by a combination of iodometric and thermogravimetric analysis. We have made use of the c/a calibration data to check the nominal δ values expected from the annealing conditions. The values of c/a, determined by neutron diffraction, and δ for the crystals studied in the present work are listed in Table I. (It should be noted that the lattice parameter values reported in the next section may have significant absolute errors due to wavelength calibration errors; nevertheless, the *ratio* c/a should be quite reliable.)

The neutron scattering experiments were performed on various triple-axis spectrometers at the High Flux Beam Reactor at Brookhaven National Laboratory. The monochromator and analyzer crystals were pyrolytic graphite (PG), with the monochromator, and usually the analyzer, set for the (002) reflection. A wide range of spectrometer configurations was used for the diffraction work. On the thermal-neutron spectrometers H7 and H8, 14.7 meV neutrons were used with two PG filters to eliminate $\lambda/2$ and $\lambda/3$ contamination. To measure weak features such as superlattice peaks, typical horizontal collimations were 40′-40′-40′-40′, whereas for fundamental reflections the collimations were generally tightened to 10′-10′-10′-10′, together with setting the analyzer to (004). At H9, which is located on the cold-neutron source, 5.0 meV neutrons were used to study weak features, and 3.5 meV for higher resolution. In both cases, a Be filter was employed to remove higher harmonics.

TABLE I. Values of c/a and oxygen excess δ for the various single-crystal samples. The numbers in parentheses indicate the estimated uncertainty in the last digit of the corresponding parameter values.

Sample No.	c/a	δ
LN9	2.3028(10)	0.058(3)
LN14	2.3047(10)	0.060(3)
LN11	2.3088(15)	0.074(4)
LN12	2.3094(15)	0.085(4)
LN8	2.3114(10)	0.105(3)

Each $La_2NiO_{4+\delta}$ crystal was wrapped in Al foil, attached to a thin Al disk on a sample holder, and sealed in an Al can with He exchange gas. Exposure to the ambient atmosphere was minimized to avoid unintended changes in oxygen content. Before sealing the sample can, each sample was oriented with an orthorhombic [010]/[100] axis vertical to allow the study of scattering in the $(h0l)/(0kl)$ zone. Sample temperature was controlled with a Displex closed-cycle He refrigerator, and the temperature was monitored with either a Pt resistance thermometer or a Si diode attached to the cold finger. For rapid cooling (quenching), the Displex was simply allowed to cool, without interruption, from 300 K to 200 K. The maximum cooling rate achieved was 3 K/min.

IV. RESULTS

Crystals with $\delta = 0.058$, 0.06, 0.074, 0.085, and 0.105 were studied in the present work. Rather than describing the results in order of increasing δ, we choose to present them in order of increasing complications. Thus, we begin with $\delta = 0.105$, where the oxygen ordering appears to yield an essentially single-phase stage-2 structure. This is followed by the $\delta = 0.074$ sample, which exhibits a phase separation, on slow cooling, into stage-2 and stage-3 domains. Finally, we describe the $\delta = 0.06$ crystal, which shows phase separation into the $P4_2/ncm$ phase and an intercalated structure involving a random stacking of stage-3 and stage-4 units. The samples with $\delta = 0.058$ and 0.085 did not show any qualitatively new behavior, and so no details concerning them will be given.

A. $\delta = 0.105$

In our original study[16] of the $\delta = 0.105$ crystal, we observed that, on cooling below ~ 290 K, an orthorhombic phase grew out of the HTT phase that occurs at room temperature.[6] The kinetics of the transition were quite slow, consistent with diffusion of oxygen ions. We incorrectly interpreted this behavior, together with the incomplete conversion from tetragonal to orthorhombic, as evidence of phase separation into low δ and high δ phases. Associated with the orthorhombic phase are superlattice peaks at positions $(0, k, l \pm \Delta)$ with k odd, l even, and $\Delta \approx \frac{1}{2}$. In the earlier work,[16] we did not notice the fact that Δ is not exactly equal to $\frac{1}{2}$. (The cause of the discrepancy will be explained shortly.) Nevertheless, a reasonable model for the structure was proposed: The superlattice peaks are caused by the tilt pattern of the NiO_6 octahedra, which involves a doubling of the unit cell along c. The report of much larger unit cells associated with oxygen ordering in the electron diffraction study by Hiroi *et al.*[12] led us to conclude, incorrectly, that the superlattice peaks were not caused by the interstitials, but rather by a charge-density-wave ordering. However, a large accumulation of evidence now makes it clear that the cell doubling is associated with a one-dimensional (1D) ordering of intercalated oxygen.

An important clue to the nature of the structural transition comes from the diffuse scattering that is observed along the $(0,1,l)$ and $(0,3,l)$ rods above the transition. The l dependence of the intensity is qualitatively consistent with the structure factor for a single unit cell (along c) of the low-temperature orthorhombic phase (see Fig. 2 of Ref. 16). The scattering perpendicular to the rods is much more sharply peaked, as illustrated in Fig. 5. It can be modeled in terms of a narrow Gaussian peak plus a broad one. The narrower component has a width comparable to the orthorhombic splitting found in the low-temperature phase. The correlation length for the atomic displacements is clearly much longer in the directions parallel to the planes than it is in the perpendicular direction. These observations are consistent with what one might expect for lamellar clusters of intercalated oxygens, with only weak correlations along c between the clusters. The tilts of the NiO_6 octahedra induced by the interstitial oxygens may cause the local symmetry to be orthorhombic, but an incoherent averaging of such regions would yield an average tetragonal symmetry.

To better characterize the structural transition, we monitored the (200) diffraction peak as the crystal was slowly cooled, in a stepwise fashion, from room temperature. Typical scans of the (200) region are displayed in Fig. 6; the time dependence of the integrated intensities is shown in Fig. 7, and the temperature dependence of the lattice parameters is plotted in Fig. 8. After cooling to 290 K and waiting for several hours, the (200) and (020) peaks of the orthorhombic phase began to appear. While the intensities of the two peaks grew gradually with time, their positions did not change. Somewhat surprisingly, the intensity of the tetragonal (200) peak remained constant during this time. After 6 h, the temperature was reduced to 285 K. The intensities of the orthorhombic peaks initially grew quite rapidly, and the tetragonal peak began to decrease. The time dependence of the peaks following the stepwise temperature changes was followed down to 240 K. No significant change in the relative peak intensities was observed below 260 K.

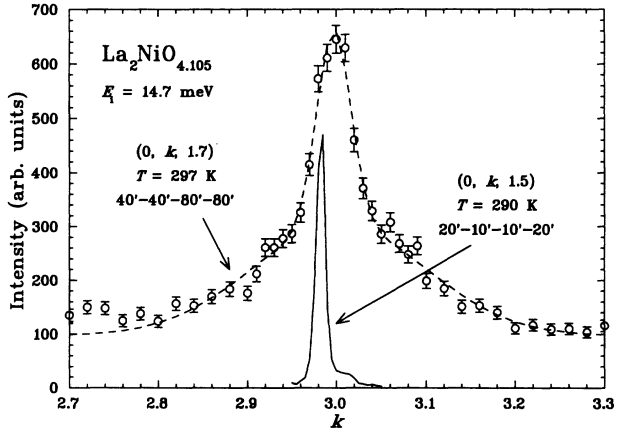

FIG. 5. Open circles: Scan along $Q = (0,k,1.7)$ through the diffuse scattering that runs along the $(3,0,l)$ and $(0,3,l)$ rods in the disordered state of $La_2NiO_{4.105}$, measured at a temperature of 297 K with coarse collimation. The dashed line is a fit with two Gaussian peaks, one narrow and one broad, and a background level of 95. Solid line: Scan along $(0,k,1.5)$ through the superlattice peak due to oxygen ordering at 290 K, measured with tight collimation and with the calibration such that $k = 3$ corresponds to the tetragonal phase. It is included to indicate the magnitude of the orthorhombic splitting.

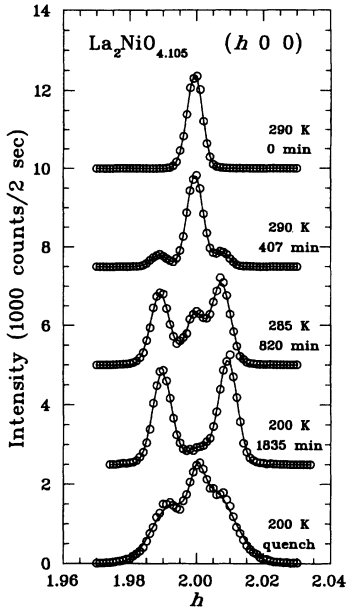

FIG. 6. Scans of the (200) peak in $La_2NiO_{4.105}$ measured using $E_i = 3.5$ meV and effective horizontal collimations 20'-40'-20'-20' during the slow cooling cycle discussed in the text. Sample temperature and time from the start of the cycle are indicated for each scan. In the orthorhombic phase, the (200) and (020) peaks are observed simultaneously due to twinning. The bottom curve was measured after quenching from 300 K to 200 K.

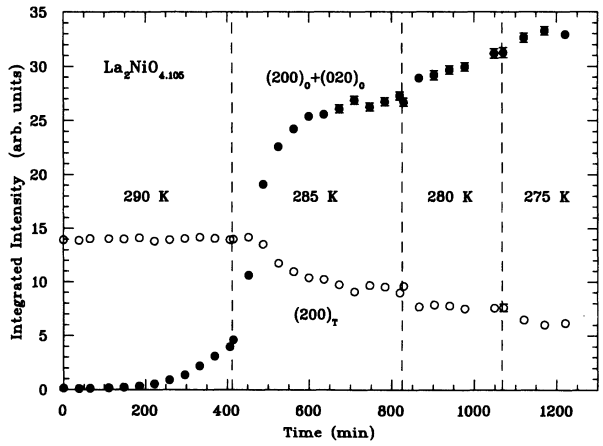

FIG. 7. Integrated intensities of the (200) peaks (such as those shown in the previous figure) as a function of time during the slow cooling cycle discussed in the text. For the orthorhombic phase, the sum of the (200) and (020) intensities is plotted. Dashed lines indicate the times at which the temperature was lowered; temperature was held constant at the indicated values during the intervening intervals.

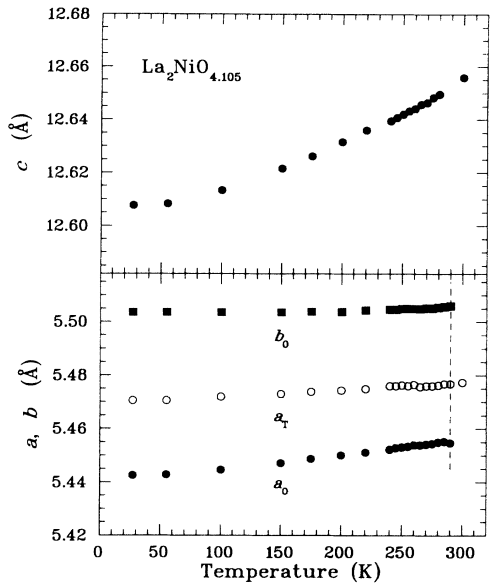

FIG. 8. Temperature dependence of the lattice constants in $La_2NiO_{4.105}$.

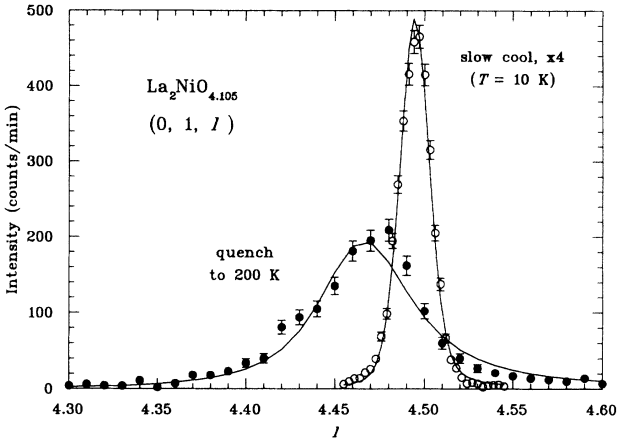

FIG. 9. Scans through the superlattice peak near (0,1,4.5) in the $\delta = 0.105$ crystal measured after slow cooling (open circles) and after quenching from 300 K to 200 K (solid circles). Solid lines are fits assuming random ordering of stage-2 and stage-3 components, with $f_{2:2} = 0.933$, $f_{3:3} = 0$ for the slow cool data; $f_{2:2} = 0.676$, $f_{3:3} = 0.069$ for the quench.

The tetragonal-to-orthorhombic transitions typically seen in the layered perovskites, such as the HTT-to-LTO transition in $La_{2-x}Sr_xCuO_4$, are second order, with a continuous increase in the orthorhombic strain below the transition. In contrast, the temperature dependence of the a and b lattice parameters shown in Fig. 8 indicates a negligible change in the orthorhombic strain for $La_2NiO_{4.105}$. The observation of a unique c lattice parameter at each temperature argues against phase separation, since c is known to vary considerably with δ.[6] The data clearly suggest that the transition involves an ordering of the preexisting lamellar clusters. The slow kinetics indicate that the ordering is limited by diffusion of the interstitial oxygens.

Since the ordering occurs so slowly, one might imagine that a good deal of disorder could be frozen in by rapid cooling. The bottom curve in Fig. 6 shows the result of quenching the crystal from 300 K to 200 K. A large amount of the tetragonal phase remains, and the orthorhombic peaks are quite broad. The width indicates a domain size on the order of 40 lattice spacings perpendicular to the c axis. This is at least 3 times smaller than the domain size obtained by slow cooling. The finite domain dimension in this direction is consistent with ordering involving diffusion of the interstitials parallel to the planes.

The superlattice peaks provide another window on the ordering. A measurement of the peak near $(0, 1, 4 + \Delta)$ with $\Delta \approx \frac{1}{2}$, obtained after slow cooling, is shown in Fig. 9. Measurements on a series of superlattice peaks confirms that Δ is actually 0.494, rather than 0.5 as one would expect for perfect stage-2 ordering. The deviation can be explained by allowing for some disorder in the layer stacking. The solid line in the figure is a fit to the data using the Hendricks-Teller formulas, discussed earlier, for a random stacking of layers, which we assume to be stage-2 and stage-3 units. The fit corresponds to $f_{2:2} = 0.933$, $f_{3:3} = 0$, and $f_{2:3} = 0.033$. A small fraction of stage-3 defects gives a quite observable displacement of the peaks. Quenching the sample causes a much more substantial displacement and broadening of the superlattice peaks, as demonstrated in Fig. 9. The solid line is a fit that yields $f_{2:2} = 0.676$ and $f_{3:3} = 0.069$, indicating a large increase in stacking errors compared to the slow-cool case. A more detailed study of the time and temperature dependence of the superlattice peaks will be reported elsewhere.[24]

One last feature of the low-temperature phase deserves mention. Because of the B-centered symmetry of the $Bmab$ structure, reflections such as $(h0l)$ with h even and l odd [and $(0kl)$ with k even and l odd] have zero intensity. However, we observe weak but finite intensity at these positions (see Fig. 3) whenever the orthorhombic phase with $\Delta \approx \frac{1}{2}$ is present. This is further evidence for the stage-2 intercalated $Bmab$ structure, since the interstitial oxygens should cause a slight expansion of the occupied La_2O_2 layers, which breaks the B-centered symmetry.

B. $\delta = 0.074$

It has taken quite some time to understand this sample, because not only is there a transition involving ordering of the intercalated layers, but there is also a phase separation into regions with different orderings. The proper interpretation only became clear after the concept of staging was developed. The problem is illustrated by the superlattice peak measurements shown in Fig. 10. On slow cooling (lower panel), one observes two peaks corresponding to $\Delta \approx \frac{1}{2}$ and $\frac{1}{3}$, whereas quenching results in a single peak at a somewhat intermediate position. These features are readily interpreted with the intercalated-$Bmab$

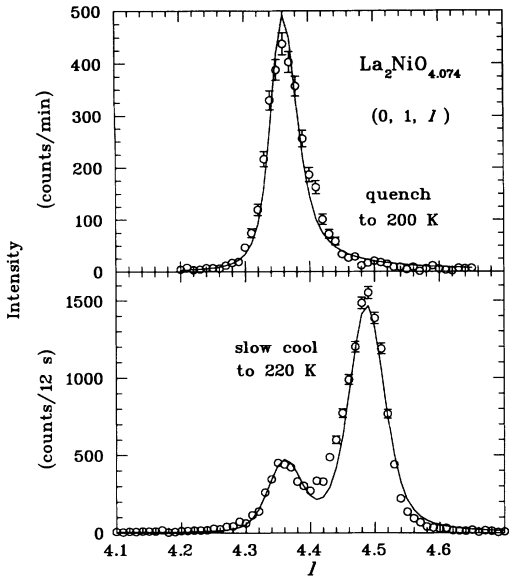

FIG. 10. Scans near the (0,1,4.5) position for the $\delta = 0.074$ crystal. Top: Measurement after quenching from 300 K to 200 K, using $E_i = 5.0$ meV and effective horizontal collimations 30′-40′-80′-80′. Bottom: Measured at 220 K after slow cooling, using $E_i = 14.7$ meV, 40′-40′-40′-40′. The solid lines are fits assuming a random ordering of stage-2 and stage-3 components with, for the top, $f_{2:2} = 0.105$, $f_{3:3} = 0.580$; for the bottom, two phases with $f_{2:2} = 0.847$, $f_{3:3} = 0.035$ for one and $f_{2:2} = 0.053$, $f_{3:3} = 0.574$ for the other.

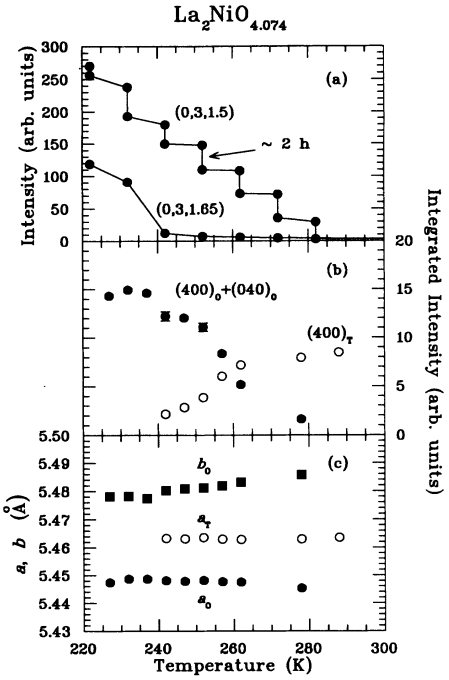

FIG. 11. Temperature dependence of various quantities measured for $La_2NiO_{4.074}$. (a) Intensity at the points (0,3,1.5) and (0,3,1.65), measured on cooling. For the (0,3,1.5) data, the time between the two measurements at a given temperature is approximately 2 h. (b) Integrated intensities of the (400) peaks of the orthorhombic and tetragonal phases, measured on warming. (c) Lattice constants for the orthorhombic and tetragonal phases.

model. The two peaks found on slow cooling indicate that both stage-2 and stage-3 phases are present, each with significant stacking disorder. A fit to the data with a two-phase model is indicated by the solid line in the lower panel of Fig. 10. Since the sample appears to be a homogeneous tetragonal phase at room temperature, phase separation must occur on cooling. The phase separation can be avoided by rapid cooling, leading to the single peak shown in the upper panel. A fit with randomly ordered stage-2 and stage-3 units is indicated by the solid line.

A complicating factor in identifying the phase separation is that the stage-2 and stage-3 phases appear at different temperatures. The temperature dependence of the intensity near the $(0, 3, 2 - \frac{1}{2})$ and $(0, 3, 2 - \frac{1}{3})$ positions is shown in Fig. 11(a). The peak corresponding to stage-2 ordering appears at 280 K, and grows gradually as the temperature decreases, with a strong time dependence of the intensity down to 220 K. The stage-3 peak first starts to grow near 250 K, but only shoots up below 240 K.

Following the transitions via the fundamental (400) and (040) reflections [see Figs. 11(b) and 11(c)], the orthorhombic splitting first appears near 280 K, with the stage-2 superlattice peak, and the intensity of the orthorhombic peaks grows gradually with decreasing temperature. The tetragonal peak does not disappear until the temperature drops below 240 K. Although we cannot resolve two different orthorhombic splittings, it is of interest that $b - a$ tends to *decrease* on cooling. We expect that the orthorhombic strain should be slightly smaller in stage-3 than in stage-2 because of the lower density of interstitials. Thus we suggest that the decrease in the splitting reflects the increasing fraction of the stage-3 phase at lower temperatures.

C. $\delta = 0.06$

A phase separation occurs at this concentration as well, but it is more easily identified because the c lattice parameters of the two phases are distinct (see Fig. 12). The crystal appears to be uniformly HTT at 300 K, but on cooling to 290 K a new tetragonal phase appears, with a larger a and smaller c. Associated with the new phase are superlattice peaks of the type $(0kl)$ with k odd and l even. The lattice parameters and the superlattice peaks identify this phase as LTT with $\delta \approx 0.025$.[6] The fraction of the sample volume in the LTT phase increases gradually until the temperature reaches 240 K, saturating at roughly 12%. The growth of the LTT fraction is reflected in the temperature dependence of the intensity of the (032) superlattice peak, shown in Fig. 13. The remaining HTT fraction appears to undergo a second-order transition to an orthorhombic phase at 250 K. The orthorhombic strain increases on cooling to 220 K, at which point the strain appears to lock in to a fixed value, and

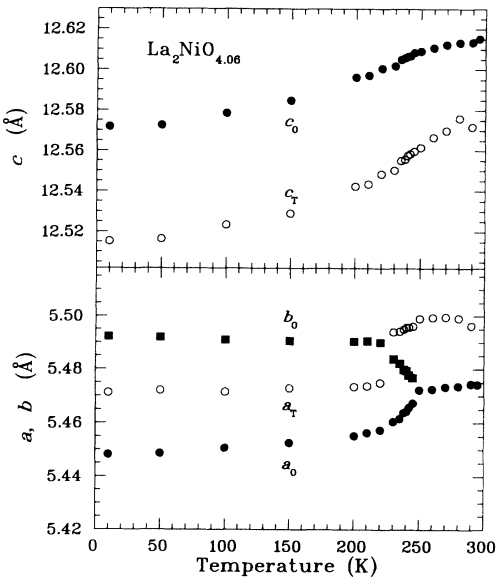

FIG. 12. Temperature dependence of the lattice parameters for the orthorhombic and tetragonal phases in $La_2NiO_{4.06}$.

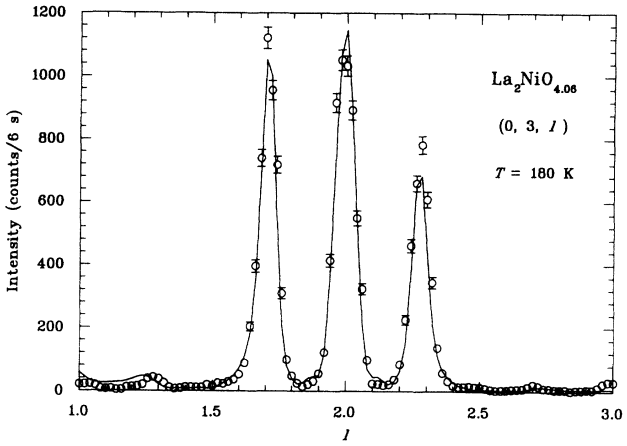

FIG. 14. Scan along $(0,3,l)$ for the $\delta = 0.06$ crystal at a temperature of approximately 180 K (open circles). The solid line is a fit assuming two phases: (1) an LTT phase, 12% by volume, to describe the (0,3,2) peak, and (2) a random ordering of stage-3 and stage-4 layers with $f_{3:3} = 0.376$, $f_{4:4} = 0.447$.

at the same time the value of a for the tetragonal phase jumps to a value commensurate with the average of the orthorhombic a and b.

Superlattice peaks associated with the orthorhombic phase appear with $\Delta \approx 0.30$, the precise value depending on the cooling rate. An example of the superlattice peaks is presented in Fig. 14. The intensities of these peaks grow quite rapidly near 235 K, and the diffuse scattering found in the HTT phase drops off quickly in the same temperature region, as shown in Fig. 13. It is interesting that the intensity of the (032) peak drops slightly when

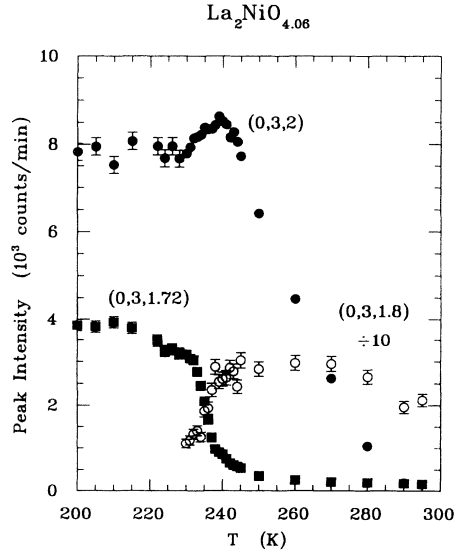

FIG. 13. Temperature dependence of the scattered intensity at three points along $(0,3,l)$ measured for the $\delta = 0.06$ crystal on cooling.

$(0,3,2-\Delta)$ undergoes its rapid growth. The coupled behavior of the intensities and lattice parameters suggests that the domains of the two phases are coherently coupled.

The superlattice peaks of the orthorhombic phase can be fit with a model involving a random stacking of stage-3 and stage-4 units, as indicated in Fig. 14. We have not been able to eliminate the LTT phase by quenching, and we have never observed a separation into distinct stage-3 and stage-4 phases. Such a separation may be kinetically inhibited.

D. Magnetic ordering

The antiferromagnetic structure of $La_2NiO_{4+\delta}$ with $\delta \approx 0.05$ (later found[25] to be $\delta = 0.067$ by iodometric titration) was first determined by Aeppli and Buttrey,[26] and shown to be identical to that in the stoichiometric $\delta = 0$ phase. The Ni spins are aligned along the [100] direction, parallel to the wave vector describing the antiferromagnetic order. As a result, the allowed magnetic Bragg peak at (100) has zero intensity for neutron diffraction, and the first strong peak is at (011). The temperature dependence of the (011) intensity observed in our $\delta = 0.06$, 0.074, and 0.105 crystals are shown in Fig. 15. For each sample the intensity was normalized to the value obtained at the lowest temperature. The normalized intensity should be equal to $M^2(T)/M^2(0)$, where $M(T)$ is the average ordered magnetic moment at temperature T. Similar results were obtained for the $\delta = 0.058$ and 0.084 crystals. For $\delta = 0.06$ (and 0.058), the Néel temperature of the dominant phase is approximately 80 K, but the (011) intensity does not go to zero at that point because of magnetic scattering from the $\delta \approx 0.025$ minority phase, which has an ordering temperature of $\sim$ 190 K. We confirmed this assignment of the Néel temperatures to the two separated phases for the $\delta = 0.058$ sample

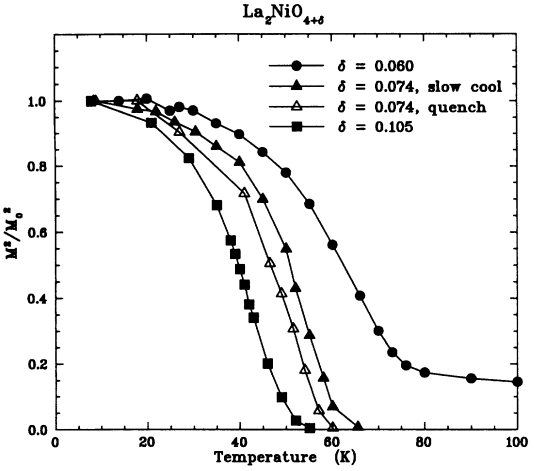

FIG. 15. Normalized square of the average ordered magnetic moment (normalized Bragg peak intensity) vs temperature for crystals with $\delta = 0.06$, 0.074, and 0.105. The two sets of data for $\delta = 0.074$ show the difference observed after slow cooling and after quenching.

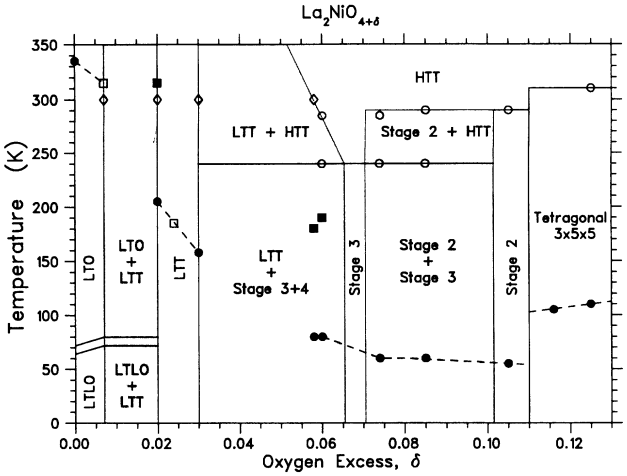

FIG. 16. Revised phase diagram for $La_2NiO_{4+\delta}$. Open circles (diamonds) indicate phase boundaries determined by neutron single-crystal (x-ray powder) diffraction. Solid circles denote Néel temperatures of primary phase, solid squares indicate Néel temperatures of secondary phases, and open squares indicate these transitions translated to the appropriate values of δ. The stage-3 phase region is an estimate—that pure phase has not yet been observed. For $0.11 \lesssim \delta \lesssim 0.13$, the interstitial oxygens are ordered three dimensionally, and the incommensurate magnetic ordering involves a simultaneous ordering of holes.

by studying the magnetic (017) reflection with high resolution, and identifying the two contributions by their distinct values of c^*.

The Néel temperatures that we have observed are consistent with previous work.[7,26,25] One new feature is that we find a small dependence of T_N on the degree of oxygen ordering, as controlled by cooling rate, for the $\delta = 0.074$ sample. We have looked for evidence of extra magnetic peaks along the $(01l)$ direction, which might be associated with the periodic ordering of the interstitials, but we have found none. We have also found no evidence for the incommensurate magnetic peaks that are observed in the $\delta = 0.125$ phase.[27,28] We did once observe weak diffuse scattering centered at (100) in the $\delta = 0.105$ crystal at low temperature, but it disappeared after cycling through T_N. A systematic study of that feature has not been performed.

V. DISCUSSION

Our results are summarized by the phase diagram shown in Fig. 16. We have made substantial revisions in the region $0.03 < \delta < 0.13$ and $T < 300$ K, compared to our earlier versions.[6,16] The indicated stage-3 phase is only a speculation at this point, as a pure stage-3 ordering has not yet been observed. (However, it is interesting to note that the $\delta = 0.067$ crystal studied previously[25] exhibited a single tetragonal-to-orthorhombic transition near 235 K, consistent with the proposed stage-3 phase.) Although we have indicated only our own results[6,16,28,29] in the figure, a number of the phase boundaries, especially at low δ, are confirmed by the work of other groups.[7,8,23,30–33] For $\delta \gtrsim 0.11$, incommensurate magnetic ordering at $\delta = 0.125$ was first identified by Yamada *et al.*[27] In a separate study,[28] we confirmed that result, demonstrated that the electronic holes induced by the oxygen doping order simultaneously with the Ni spins, and presented evidence that the interstitial oxygens order three dimensionally below ~ 310 K, with a unit cell of size $3 \times 5 \times 5$ relative to LTO. A point is also included on the phase diagram for a $\delta = 0.116$ crystal that has been only partially characterized.

We believe that our model of the intercalated *Bmab* phase is consistent with the neutron powder diffraction work of Jorgensen *et al.*[9] The Rietveld refinement method used in the latter work puts a very large weight on the strong fundamental reflections; it gives a good description of the overall symmetry and the average positions of the atoms within a fundamental unit cell. On the other hand, the identification of staging of the intercalated layers in the present work relies on detection and analysis of the very weak superlattice peaks, recognition of the slow ordering kinetics, and an accurate control and characterization of the oxygen excess, δ. For $\delta \lesssim 0.11$, we have not observed any evidence for three-dimensional ordering of the interstitials, contrary to the results of the electron diffraction study by Hiroi *et al.*[12] The differences are actually quite significant, because the 1D ordering that we observe occurs below 290 K, whereas the electron diffraction work appears to have been done at ambient temperature, which would be $\gtrsim 300$ K taking beam heating into account. It is possible that the interstitial oxygens order differently in the extremely thin crystals required for electron microscopy than they do in the large crystals studied with neutrons, but it is also possible that the oxygen concentrations of the individual crystallites studied in the electron microscope are different from the nominal values. A measurement of the c/a ratio of the

fundamental lattice associated with each superstructure would provide a useful test.

The periodic ordering of interstitial layers in $La_2NiO_{4+\delta}$ seems quite similar to the staging of graphite intercalated with alkali atoms. The ordering behavior in graphite can largely be explained by 1D models involving repulsive interactions between the alkali layers.[17] In such models, there tends to be a unique 1D ordering of full and empty layers for each concentration of alkali atoms. The fact that we observe temperature-dependent phase separations in $La_2NiO_{4+\delta}$ indicates that a proper model for this system must also include interactions within the layers. To explain the clustering of the interstitial oxygen ions in layers, as observed above the ordering transition, a significant attractive interaction is required in order to overcome the Coulomb repulsion. It is possible that the clustering and phase separation are driven by the interactions between the electronic holes, as suggested by Emery and Kivelson[34] in the case of $La_2CuO_{4+\delta}$. Further analysis of this problem will be discussed elsewhere.[35]

The phase separations and slow ordering kinetics that are found in $La_2NiO_{4+\delta}$ seem rather similar to the behaviors observed in $La_2CuO_{4+\delta}$.[3–5,11,36–43] We suggest that 1D ordering of the oxygen interstitials may also occur in $La_2CuO_{4+\delta}$. It is of interest to search for $(0, k, l\pm\Delta)$-type superlattice peaks in single crystals with δ in the phase separation regime. Radaelli *et al.*[15] have found a very complicated superlattice structure in a nominally single-phase single crystal with $\delta \sim 0.1$; however, that might be beyond the regime of 1D order. A complicated superstructure is also observed in $La_2NiO_{4+\delta}$ with $\delta > 0.11$.[28]

While the main focus of the present paper has been on the oxygen ordering, we also wish to comment on the effects of the hole doping on the magnetic order. In comparison with the cuprates, the rather gradual reduction of T_N with increasing δ is much more similar to the behavior observed in electron-doped $Nd_{2-x}Ce_xCuO_4$ than that in hole-doped $La_{2-x}Sr_xCuO_4$, where the magnetic order drops to zero by $x = 0.02$.[44] The differences between the electron- and hole-doped systems have been discussed in terms of the effective orbital size associated with the added electrons or holes in the antiferromagnetic regime.[45,46] Applying these arguments to $La_2NiO_{4+\delta}$, it appears that, at least in terms of the magnetic order, the holes behave as if they are quite localized.

The discovery[28] of a complementary ordering of holes and spins for $\delta > 0.11$ leads to new questions concerning the magnetism for $\delta < 0.11$. Why does the magnetic order change so abruptly from commensurate to incommensurate (or long-period commensurate) near $\delta = 0.11$? Is it associated with the change from 1D to 3D ordering of the oxygen interstitials? Can the effects of the interaction between holes and spins be detected in the spin dynamics for $\delta < 0.11$? Clearly, there are many interesting questions left to study.

Note added: Very recently, Yazdi *et al.*[47] have completed a study of electrochemical intercalation of oxygen in polycrystalline $La_2NiO_{4+\delta}$ at a temperature of 273 K. Their results suggest single-phase regions that are reasonably consistent with the stage-2 and stage-3 phases indicated in Fig. 16. In addition, they find evidence for a distinct phase centered at $\delta = 0.087$. We hope to investigate this feature collaboratively in a future study on an electrochemically prepared single crystal.

ACKNOWLEDGMENTS

We gratefully acknowledge helpful discussions with J. D. Axe, P. Bak, V. J. Emery, U. Löw, G. Shirane, and D. O. Welch. Special thanks go to T. R. Thurston for his assistance with some of the experimental measurements. Work at Brookhaven was carried out under Contract No. DE-AC02-76CH00016, Division of Materials Sciences, U.S. Department of Energy. D.J.B., D.E.R., and V.S. acknowledge support from the National Science Foundation under Contract No. DMR-8914080.

* Present address: X-Ray Instrumentation Associates, 2513 Charleston Rd., Suite 207, Mountain View, CA 94043.

[1] J. G. Bednorz and K. A. Müller, Z. Phys. B **64**, 189 (1986).
[2] P. M. Grant, S. S. P. Parkin, V. Y. Lee, E. M. Engler, M. L. Ramirez, J. E. Vazquez, G. Lim, R. D. Jacowitz, and R. L. Greene, Phys. Rev. Lett. **58**, 2482 (1987).
[3] J. D. Jorgensen, B. Dabrowski, S. Pei, D. G. Hinks, L. Soderholm, B. Morosin, J. E. Schirber, E. L. Venturini, and D. S. Ginley, Phys. Rev. B **38**, 11337 (1988).
[4] M. F. Hundley, J. D. Thompson, S. Cheong, Z. Fisk, and J. E. Schirber, Phys. Rev. B **41**, 4062 (1990).
[5] P. C. Hammel, A. P. Reyes, Z. Fisk, M. Takigawa, J. D. Thompson, R. H. Heffner, S. Cheong, and J. E. Schirber, Phys. Rev. B **42**, 6781 (1990).
[6] D. E. Rice and D. J. Buttrey, J. Solid State Chem. **105**, 197 (1993).
[7] S. Hosoya, T. Omata, K. Nakajima, K. Yamada, and Y. Endoh, Physica C **202**, 188 (1992).
[8] H. Tamura, A. Hayashi, and Y. Ueda, Physica C **216**, 83 (1993).
[9] J. D. Jorgensen, B. Dabrowski, S. Pei, and D. G. Hinks, Phys. Rev. B **40**, 2187 (1989).
[10] C. Chaillout, S. W. Cheong, Z. Fisk, M. S. Lehmann, M. Marezio, B. Morosin, and J. E. Schirber, Physica C **158**, 183 (1989).
[11] C. Chaillout, J. Chenavas, S. W. Cheong, Z. Fisk, M. Marezio, B. Morosin, and J. E. Schirber, Physica C **170**, 87 (1990).
[12] Z. Hiroi, T. Obata, M. Takano, Y. Bando, Y. Takeda, and O. Yamamoto, Phys. Rev. B **41**, 11665 (1990).
[13] A. Demourgues, F. Weill, B. Darriet, A. Wattiaux, J. C. Grenier, P. Gravereau, and M. Pouchard, J. Solid State Chem. **106**, 317 (1993).
[14] A. Demourgues, F. Weill, B. Darriet, A. Wattiaux,

J. C. Grenier, P. Gravereau, and M. Pouchard, J. Solid State Chem. **106**, 330 (1993).
[15] P. G. Radaelli, J. D. Jorgensen, A. J. Schultz, B. A. Hunter, J. L. Wagner, F. C. Chou, and D. C. Johnston, Phys. Rev. B **48**, 499 (1993).
[16] J. M. Tranquada, D. J. Buttrey, and D. E. Rice, Phys. Rev. Lett. **70**, 445 (1993).
[17] S. Safran, Solid State Phys. **40**, 183 (1987).
[18] C. D. Fuerst, J. E. Fischer, J. D. Axe, J. B. Hastings, and D. B. McWhan, Phys. Rev. Lett. **50**, 357 (1983).
[19] M. E. Misenheimer and H. Zabel, Phys. Rev. Lett. **54**, 2521 (1985).
[20] J. D. Axe (private communication).
[21] S. Hendricks and E. Teller, J. Chem. Phys. **10**, 147 (1942).
[22] J. Kakinoki and Y. Komura, J. Phys. Soc. Jpn. **7**, 30 (1952).
[23] G. H. Lander, P. J. Brown, J. Spałek, and J. M. Honig, Phys. Rev. B **40**, 4463 (1989).
[24] J. E. Lorenzo, J. M. Tranquada, D. J. Buttrey, and V. Sachan (unpublished).
[25] T. Freltoft, D. J. Buttrey, G. Aeppli, D. Vaknin, and G. Shirane, Phys. Rev. B **44**, 5046 (1991).
[26] G. Aeppli and D. J. Buttrey, Phys. Rev. Lett. **61**, 203 (1988).
[27] K. Yamada, T. Omata, K. Nakajima, Y. Endoh, and S. Hosoya, Physica C **221**, 355 (1994).
[28] J. M. Tranquada, D. J. Buttrey, V. Sachan, and J. E. Lorenzo (unpublished).
[29] D. J. Buttrey, D. E. Rice, V. Sachan, and J. M. Tranquada (unpublished).
[30] J. Rodríguez-Carvajal, J. L. Martínez, J. Pannetier, and R. Saez-Puche, Phys. Rev. B **38**, 7148 (1988).
[31] T. Kajitani, Y. Kitagaki, K. Hiraga, S. Hosoya, T. Fukuda, Y. Yamaguchi, S. Wada, S. Sugai, Y. Morii, K. Fuchizaki, and S. Funahashi, Physica C **185**, 579 (1991).
[32] J. Rodríguez-Carvajal, M. T. Fernández-Díaz, and J. L. Martínez, J. Phys. Condens. Matter **3**, 3215 (1991).
[33] K. Yamada, T. Omata, K. Nakajima, S. Hosoya, T. Sumida, and Y. Endoh, Physica C **191**, 15 (1992).
[34] V. J. Emery and S. A. Kivelson, Physica C **209**, 597 (1993).
[35] U. Löw and J. M. Tranquada (unpublished).
[36] P. Zolliker, D. E. Cox, J. B. Parise, E. M. McCarron III, and W. E. Farneth, Phys. Rev. B **42**, 6332 (1990).
[37] J. Ryder, P. A. Midgley, R. Exley, R. J. Beynon, D. L. Yates, L. Afalfiz, and J. A. Wilson, Physica C **173**, 9 (1991).
[38] J. Grenier, N. Lagueyte, A. Wattiaux, J. Doumerc, P. Dordor, J. Etourneau, M. Pouchard, J. B. Goodenough, and J. S. Zhou, Physica C **202**, 209 (1992).
[39] E. T. Ahrens, A. P. Reyes, P. C. Hammel, J. D. Thompson, P. C. Canfield, Z. Fisk, and J. E. Schirber, Physica C **212**, 317 (1993).
[40] R. K. Kremer, V. Hiznyakov, E. Sigmund, A. Simon, and K. A. Müller, Z. Phys. B **91**, 169 (1993).
[41] P. C. Hammel, A. P. Reyes, S. Cheong, Z. Fisk, and J. E. Schirber, Phys. Rev. Lett. **71**, 440 (1993).
[42] P. G. Radaelli, J. D. Jorgensen, R. Kleb, B. A. Hunter, F. C. Chou, and D. C. Johnston, Phys. Rev. B **49**, 6239 (1994).
[43] D. Vaknin, J. L. Zaretsky, D. C. Johnston, J. E. Schirber, and Z. Fisk, Phys. Rev. B **49**, 9057 (1994).
[44] H. Takagi, Y. Tokura, and S. Uchida, Physica C **162-164**, 1001 (1989).
[45] M. Matsuda, Y. Endoh, K. Yamada, H. Kojima, I. Tanaka, R. J. Birgeneau, M. A. Kastner, and G. Shirane, Phys. Rev. B **45**, 12548 (1992).
[46] B. Keimer, A. Aharony, A. Auerbach, R. J. Birgeneau, A. Cassanho, Y. Endoh, R. W. Erwin, M. A. Kastner, and G. Shirane, Phys. Rev. B **45**, 7430 (1992).
[47] I. Yazdi, S. Bhavaraju, J. F. DiCarlo, D. P. Scarfe, and A. J. Jacobson (unpublished).

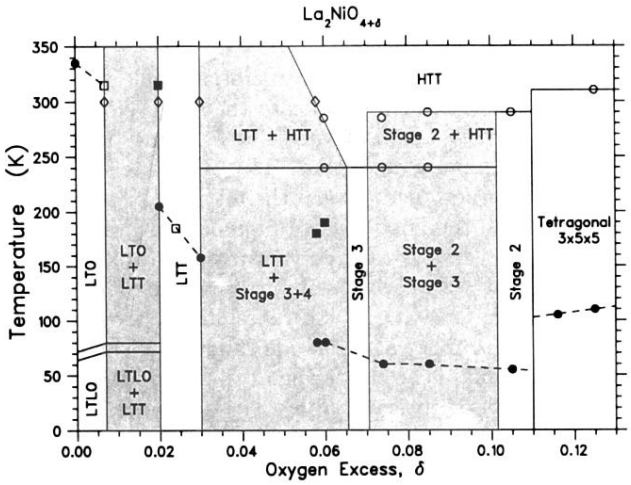

FIG. 16. Revised phase diagram for $La_2NiO_{4+\delta}$. Open circles (diamonds) indicate phase boundaries determined by neutron single-crystal (x-ray powder) diffraction. Solid circles denote Néel temperatures of primary phase, solid squares indicate Néel temperatures of secondary phases, and open squares indicate these transitions translated to the appropriate values of δ. The stage-3 phase region is an estimate—that pure phase has not yet been observed. For $0.11 \lesssim \delta \lesssim 0.13$, the interstitial oxygens are ordered three dimensionally, and the incommensurate magnetic ordering involves a simultaneous ordering of holes.